A Stochastic Computational Model for Solute Transport in Porous Media

8.1   Introduction

Computational models can often be used to investigate the phenomena it describes through experimentation with the model. In this chapter, we develop a model that describes the solute dispersion in a porous medium saturated with water considering velocity of the solute as a fundamental stochastic variable. When we consider the hydrodynamic dispersion of a solute in flowing water in a porous medium, there are two ways the solute gets distributed over the medium. The solute can mechanically disperse due to fingering effects of the granular medium and it can diffuse due to solute concentration differences. In deriving the advection-dispersion equation for solute transport, the dispersive transport is modeled by using a Fickian assumption which gives rise to the hydrodynamic dispersion coefficient (Fetter, 1999). We have seen how the perturbation term of the velocity, gives rise to the dispersive flux in Chapter 1 (section 1.3.2) and then the flux term is assumed to be related to the concentration gradient on plausibility arguments. The hydrodynamic dispersion coefficient has been found to be dependent on the scale of the experiment. The hydrodynamic dispersion contributes to making the velocity of solute particles a random variable by changing direction and magnitude in an unpredictable manner. In this chapter, we develop a model that addresses this fundamental nature of the dispersion phenomenon in porous media.

The basic assumption on which this model is based is that the velocity of solute particles is fundamentally a stochastic variable, with irregular but continuous realizations. Given the observations of Rashidi et al. (1996), this is a reasonable hypothesis. If we hypothese that the velocity constitutes of component representing mean and/or a typical value, and a fluctuating

component which depends on the characteristics of the irregular geometry of the porous medium, we can express velocity similar to equation (6.1):

$$\underline{v}(\underline{x},t) = \bar{v}(\underline{x},t) + \underline{w}(\underline{x},t). \tag{6.1}$$

$\bar{v}(\underline{x}, t)$ can be expressed as a Darcian description or as a "typical" average value of velocity for the region considered. However, we need to understand the interplay between $\bar{v}(\underline{x},t)$ and $\underline{w}(\underline{x},t)$, and the spatial region can change the value of $\bar{v}(\underline{x},t)$, and in extreme heterogeneous case, we can use $\underline{w}(\underline{x},t)$ to model the velocity recognizing that $\bar{v}(\underline{x},t)$ may not meaningfully exist. Once we have recognized this, the variables such as solute flux associated with solute transport must be treated as stochastic variables, and we need to derive the mass conservation for the solute transport problem based on theories in stochastic calculus.

8.2   Development of a Stochastic Model

We proceed to develop the model using the simplest setting possible, and for this purpose we use 1-D domain [0,a] and we keep solute concentration at x=0 at a constant value. Let us consider a 1-dimensional problem of a solute dispersion in a saturated porous medium. Consider concentration $C(x,t)$ as a stochastic variable with , for example, g/m^3 as units, $V(x,t)$ is the velocity (m/h), φ is the porosity of the material and $J(x,t)$ is the contaminant flux at x in $g/m^2.h$. As C, V, and J are stochastic functions of space and time having irregular (sometimes highly irregular) and continuous realizations, it is important to consider higher order terms to the Taylor series expansion when formulating the mass conservation model for the solute. Consider an infinitesimal cylindrical object having a cross sectional area, A (Figure 8.1).
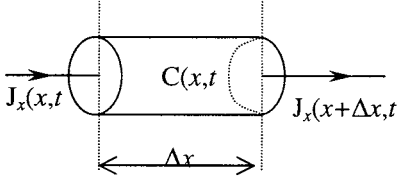
Figure 8.1   An infinitesimal cylindrical object within the porous medium having the solute concentration of $C(x,t)$.

Writing the mass balance for the change in solute during a small time increment, Δt,

$$\Delta C(x,t) \ \varphi A \ \Delta x = \left(J_x(x,t) - J_x(x+\Delta x,t) \right) \ \varphi A \ \Delta t,$$

(8.1)

$$\left(\frac{\Delta C}{\Delta t} \right)_{x,t} = \frac{\left(J_x(x,t) - J_x(x+\Delta x,t) \right)}{\Delta x}.$$

For convenience, let us indicate $J_x(x,t)$ as J_x and $J_x(x+\Delta x,t)$ as $J_{x+\Delta x}$. From the Taylor series expansion,

$$J_{x+\Delta x} - J_x = \frac{1}{1!} \frac{\partial J_x}{\partial x} \ \Delta x + \frac{1}{2!} \frac{\partial^2 J_x}{\partial x^2} \ (\Delta x)^2 + \frac{1}{3!} \frac{\partial^3 J_x}{\partial x^3} \ (\Delta x)^3 + R(\varepsilon)$$

where $R(\varepsilon)$ is the remainder of the series.

Assuming that the higher order derivatives greater than 3 of the flux are negligible, equation (8.1) can be written as

$$\frac{\partial C}{\partial t} = -\frac{\partial J_x}{\partial x} - \frac{1}{2} \frac{\partial^2 J_x}{\partial x^2} dx + R_c(x,t),$$

(8.2)

where,

$$R_c(x,t) = -\frac{1}{6}\frac{\partial^3 J_x}{\partial x^3}(dx)^2 - \frac{1}{24}\frac{\partial^4 J_x}{\partial x^4}(dx)^3 -$$

As the flux changes with the velocity, J can also be considered as changing rapidly within the porous medium creating dispersion of solutes. Even a slight variation of velocity would change the dispersion significantly over time; therefore, it is important to keep the non-linearity of the phenomenon intact if possible. We assume that the second order term captures non-linear behavior sufficiently. However in extreme heterogeneous situations, more higher order terms are needed to develop the computational model.

Substituting $dx = h_x$,

$$\frac{\partial C}{\partial t} = -\frac{\partial J_x}{\partial x} - \frac{h_x}{2}\frac{\partial^2 J_x}{\partial x^2} + R_c(x,t). \tag{8.3}$$

Equation (8.3) describes the mass conservation of the contaminant within the cylindrical volume ($A\Delta x$). Here we circumvent the discussion of nature of the variables. Obviously, $C(x,t)$ is an average over the cylindrical volume, but by making Δx smaller and smaller, we can think of $C(x,t)$ as a pore scale concentration representing a small region in space, but, if Δx is in the same order of magnitude as a typical grain size of the porous medium under consideration, $C(x,t)$ loses its meaning, so use of a realistic Δx for the medium considered is important.

$$dC = -\left(\frac{\partial J_x}{\partial x} + \frac{h_x}{2}\frac{\partial^2 J_x}{\partial x^2}\right) dt + R_c(x,t) \; dt.$$

Compared to the first term on the right hand side, let us assume that $R_c(x,t)dt \approx 0$. This assumption has to be tested in any given situation.

$$dC = -\left(\frac{\partial J_x}{\partial x} + \frac{h_x}{2}\frac{\partial^2 J_x}{\partial x^2}\right) dt. \tag{8.4}$$

Let us express the $J(x,t)$ term in terms of the velocity in the x direction and the concentration of the contaminant:

$$J(x,t) = V(x,t) \ C(x,t).$$ (8.5)

Now the velocity can be expressed as a stochastic quantity which is affected by the nature of the porous medium. The effects of the porous medium can be included within the noise term of the stochastic variable. We model the velocity in terms of the mean velocity and the Gaussian white noise:

$$V(x,t) = \overline{V}(x,t) + \xi(x,t).$$ (8.6a)

For the purpose of simplicity, we assume that $\overline{V}(\underline{x}, t)$ exists and we can express $\overline{V}(\underline{x},t)$ using the Darcy's Law:

$$\overline{V}(x,t) = -\frac{K(x)}{\varphi(x)} \frac{\partial p}{\partial x} \qquad \text{(Darcy's Law)}$$ (8.6b)

where

$K(x) =$ a typical value of the hydraulic conductivity in the region,
$\varphi(x) =$ the porosity of the material, and
$p =$ pressure head .

$\xi(x,t)$ is white noise correlated in space and δ-correlated in time such that

$$E[\xi(x,t)] = 0$$ (8.7)

$$E[\xi(x_1,t_2) \ \xi(x_2,t_2)] = q(x_1,x_2) \ \delta(t_1 - t_2)$$ (8.8)

$q(x_1,x_2)$ is the velocity covariance function in space and $\delta(t_1 - t_2)$ is the Dirac's delta function.

We can express equation (8.8), substituting $\Delta t = t_2 - t_1$,

$$E[\xi(x_1,t_1) \ \xi(x_2,t_1 + \Delta t)] = q(x_1,x_2)\delta(\Delta t).$$ (8.8a)

The Dirac's delta function $\delta(\tau)$ is defined so that it is zero everywhere except at $\tau = 0$ when it is infinite in such a way that

$$\int_{-\infty}^{\infty} \delta(\tau)\, d\tau = 1.$$

In equation (8.8a), we separate the velocity into two separate spatial and temporal components, and therefore, we say that $\xi(x,t)$ is correlated in space and δ- correlated in time. In practice, this means that we can include a "description" of porous medium through $q(x_1, x_2)$ and keep essentially the irregular behavior with respect to time. However, one could argue for the case where the velocity noise term ($\xi(x,t)$) is correlated both in space and time through covariance functions. In this case the difficulties in solving the subsequent mathematical and computational problems within the context of applications can be insurmountable. In addition, the correlation in space and δ- correlated in time of $\xi(x,t)$ can be justified based on plausible grounds. It allows us to model the randomness induced by the irregular geometry of the medium directly and we will be able to focus on the effects of heterogeneity of the medium.

Proceeding with the mathematical derivation by substituting equation (8.6a) into equation (8.5),

$$J(x,t) = \left(\overline{V}(x,t) + \xi(x,t) \right) C(x,t), \tag{8.9}$$

$$J(x,t) = \overline{V}(x,t)C(x,t) + C(x,t)\xi(x,t). \tag{8.10}$$

Substituting equation (8.10) into equation (8.5),

$$dC = -\frac{\partial}{\partial x}\left[\overline{V}(x,t)C(x,t) + C(x,t)\xi(x,t) \right] - \frac{h_x}{2}\frac{\partial^2}{\partial x^2}\left[\overline{V}(x,t)C(x,t) + C(x,t)\xi(x,t) \right],$$

$$= -\left(\frac{\partial}{\partial x} + \frac{h_x}{2}\frac{\partial^2}{\partial x^2} \right) * \left[\overline{V}(x,t)C(x,t) + C(x,t)\xi(x,t) \right]. \tag{8.11}$$

Let us define the operator in space,

$$S = -\left(\frac{h_x}{2}\frac{\partial^2}{\partial x^2} + \frac{\partial}{\partial x} \right) \text{ for a given } h_x.$$

Then:

$$dC = S\left(\overline{V}(x,t)C(x,t) + C(x,t)\xi(x,t)\right)dt,$$

$$dC = S\left(\overline{V}(x,t)\ C(x,t)\right)\ dt + S\left(C(x,t)\ \left(\xi(x,t)\ dt\right)\right). \tag{8.12}$$

Equation (8.12) has the form of a stochastic differential equation and both terms on the right hand side can be integrated as Ito integrals to obtain concentration. We introduce $d\beta(t) = \xi(x,t)dt$ where $\beta(t)$ is a Wiener process in Hilbert space for a given x.

Therefore equation (8.12) can be written as:

$$dC = S\left(\overline{V}(x,t)\ C(x,t)\right)\ dt + S\left(C(x,t)\ d\beta(t)\right). \tag{8.13}$$

This means in the integral notation,

$$C(x,t) = \int_o^t S\left(\overline{V}(x,t)\ C(x,t)\right)\ dt + \int_o^t S\left(C(x,t)\ d\beta(t)\right) \tag{8.14}$$

where S is the differential operator given above.

Unny (1989) showed that $d\beta(t)$ can be approximated by:

$$d\beta_m(t) = \sum_{j=1}^{m} f_j \sqrt{\lambda_j}\ db_j(t), \tag{8.15}$$

where m is the number of terms used, $db_j(t)$ is the increments of standard Wiener processes, f_j and λ_j are eigen functions and eigen values of the covariance function of the velocity, respectively.

8.3   Covariance Kernel for Velocity

Ghanem and Spanos (1991) describe the mathematical details of expressing the noise term of a stochastic variable (e.g. velocity in this case) as a Karhunnen-Loeve expansion. The central to this expansion is the choice of the covariance function (Covariance Kernel) which models the spatial correlation of the 'noise' term ($\xi(x,t)$ in equation (8.6a)). We assume an exponential covariance kernel in this work to illustrate the model development. The exponential covariance kernel is frequently used in modeling the correlation of geographical data.

The exponential covariance kernel can be given as:

$$q(x_1, x_2) = \sigma^2 e^{\frac{-y}{b}} \tag{8.16}$$

where $y = |x_1 - x_2|$, b is the correlation length and σ^2 is the variance (Ghanem and Spanos, 1991). x_1 and x_2 are any two points within the range $[0,a]$. The eigen functions (f_n) and eigen values (λ_n) of $q(x_1, x_2)$ are obtained as the solution to the following integral equation:

$$\int_0^a q(x_1, x_2) \; f_n(x_2) \; dx_2 = \lambda_n f_n \; (x_1). \tag{8.17}$$

The solutions to equation (8.17) assuming σ^2 is a constant over $[0,a]$ are given by:

$$\lambda_n = \frac{2\theta\sigma^2}{\omega_n^2 + \theta^2}, \tag{8.18}$$

where $\theta = \frac{1}{b}$ and ω_n's are the roots of the following equation:

$$\tan \omega_n a = \frac{2\omega_n \theta}{\omega_n^2 - \theta^2}. \tag{8.19}$$

The orthonormal basis functions of the Hibert space associated with the exponential kernel are the eigenfunctions given by the integral equation (8.17). Equation (8.17) can be solved to yield the following function as the n th basis function:

$$f_n(x) = \frac{1}{\sqrt{N}}\left(\sin\omega_n x + \frac{\omega_n}{\theta}\cos\omega_n x\right), \tag{8.20}$$

where

$$N = \frac{1}{2}a\left(1+\frac{\omega^2}{\theta^2}\right) - \frac{1}{4\omega}\left(1+\frac{\omega^2}{\theta^2}\right)\sin 2\omega\ a - \frac{1}{2\theta}(\cos 2\omega\ a - 1). \tag{8.20a}$$

8.4   Computational Solution

8.4.1 Numerical Scheme

The differential operator S in equation (8.12) can be expressed as a difference operator using a backward difference scheme. By dividing the interval from 0 to a on x axis into ($\underline{N}$-1) equidistant and small intervals of Δx, and the interval from 0 to t on the time axis into ($\underline{K}$-1) equidistant and small intervals of Δt, we can write the derivatives for any variable U at (k,n) point on the space-time grid (Figure 8.2).
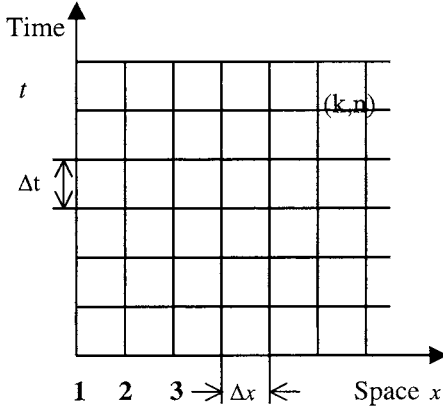
Figure 8.2   Space-time grid used in the computational scheme with respect to x.

The first derivative of a variable U can be written as

$$\left(\frac{\partial U}{\partial x}\right)_k^n = \frac{U_k^n - U_{k-1}^n}{\Delta x} \tag{8.21}$$

where U_k^n indicates the value of U at the grid point, (n,k). The second derivative can be written as

$$\left(\frac{\partial^2 U}{\partial x^2}\right)_k^n = \frac{U_k^n - 2U_{k-1}^n + U_{k-2}^n}{\Delta x^2} . \tag{8.22}$$

The operator S can be written as,

$$SU = -\left(\frac{\partial U}{\partial x} + \frac{h_x}{2}\frac{\partial^2 U}{\partial x^2}\right).$$

In the difference form

$$(SU)_k^n = -\left(\left(\frac{\partial U}{\partial x}\right)_k^n + \frac{h_x}{2}\left(\frac{\partial^2 U}{\partial x^2}\right)_k^n\right).$$

Substituting from equation (8.21) and equation (8.22) and taking $h_x = \Delta x$,

$$(SU)_k^n = -\left(\frac{1}{2\Delta x}\right)*\left[3U_k^n - 4U_{k-1}^n + U_{k-2}^n\right]. \tag{8.23}$$

The first derivative of U with respect to time can be expressed using a forward difference scheme:

$$\frac{\partial U}{\partial t} = \frac{U_k^{n+1} - U_k^n}{\Delta t}. \tag{8.24}$$

Applying equation (8.23) and (8.24) to equation (8.23) and for the case of the mean velocity (v) being constant,

$$C_k^{n+1} = C_k^n - \left(\frac{\Delta t\, v}{2\Delta x}\right)*\left[3C_k^n - 4C_{k-1}^n + C_{k-2}^n\right]$$
$$-\left(\frac{1}{2\Delta x}\right)*\left[3C_k^n\beta_k^n - 4C_{k-1}^n\beta_{k-1}^n + C_{k-2}^n\beta_{k-2}^n\right]. \tag{8.25}$$

The difference equation (8.25) gives the future value of a stochastic variable in terms of past values. In addition explicit solution procedure possesses the properties of Ito definition of integration with respect to time.

The numerical solution was implemented in Mathematica taking the numerical convergence and stability into account. The scheme has extensively been tested for 1-dimensional case, and it was found that 30 terms in equation (8.15) give a very high degree of numerical accuracy in the solution. The Mathematica program is flexible to incorporate different boundary conditions, and it was designed to test the behavior of the model with in different b and σ^2 regimes. The details of the implementation is not discussed here but are available from the authors.

8.4.2 The Behavior of the Model

As an example, we have solved equation (8.19) with $a = 1.0$m correlation length, $b = 0.05$m and obtained 11 roots: $\omega_1 = 2.85774$; $\omega_2 = 5.72555$; $\omega_3 = 8.6116$; $\omega_4 = 11.2511$; $\omega_5 = 14.4562$; $\omega_6 = 17.4166$; $\omega_7 = 23.4054$; $\omega_8 = 26.4284$; $\omega_9 = 29.4669$; $\omega_{10} = 32.5187$ and $\omega_{11} = 35.5871$. In this particular case, 11 terms in equation (8.15) is sufficient for extremely good numerical accuracy of the solution.

With these roots we have constructed the basis functions using equation (8.20). With $\sigma^2 = 1.0$ we have calculated the eigen values λ_n to construct the increments of Wiener processes in the Hilbert spaces using equation (8.15). The standard Wiener process increments were generated for $\Delta t = 0.0001$ days for a total time of 1 day (see Kloeden and Platen (1991)). The value of 50.0 m/day was used for the hydraulic conductivity and piezometric head gradient of 0.020 m/m was used to obtain the mean velocity of 4.0 m/day for a porous medium having porosity of 0.25. A realization of the solution is given in Figure 8.3.
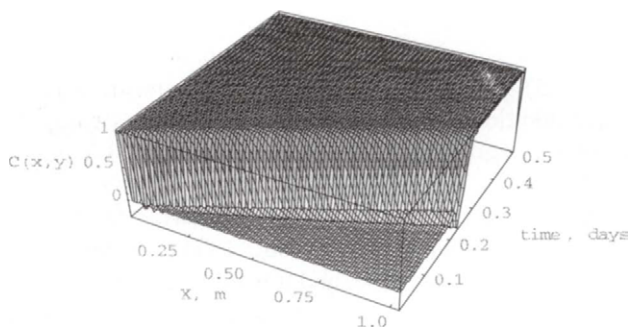
Figure 8.3   A realization of the computational solution.

The statistical nature of the computational solution changes as σ^2 and b change. This allows us to model hydrodynamic dispersion without the need for a scale dependent diffusion coefficient. In this example, we have a very high value for the mean velocity and as a result we can expect advection to dominate as seen in this example; therefore, high stochastic amplitude of 1.0 does not have a significant effect on the realization. Next we will use a simplistic setting to examine the behavior of the model to gain some insight as to how σ^2 and b influence hydrodynamic dispersion.

To illustrate the behavior of the model, we solved the 1-dimensional problem for the domain $0 \leq x \leq 1$ with a constant concentration of 1.0 applied at the boundary x = 0. Then we obtained the temporal development of the concentration profile at the mid point of the domain $x = 0.5$ for various combinations of σ^2 and b and we have kept all other parameters constant: the mean velocity was taken to be 0.5 m/day and we have used the same standard Wiener increments for all the experiments. Qualitative nature of our understanding about how the model behaves proved to be independent of the particular realization of the Wiener process.

8.5   Computational Investigation

We have   investigated the Stochastic Solute Transport Model (SSTM) described in the previous section for simple settings of one-dimensional case to understand its behavior. The main parameters of the model are the correlation length, b and the variance, σ^2. As the statistical nature of the computational solution changes with b and σ^2, the main objective of this exercise is to identify effects of these parameters to the solution of the model.

The distributed concentration values were obtained by using the finite difference numerical solution taking the numerical convergence and stability into consideration. We first illustrate the behavior of the model by solving one-dimensional problem for the spatial domain of 1 m ($0 \leq x \leq 1$). We solved equation (8.19) to generate the roots for a given set of parameters. For an instance, for the correlation length, $b = 0.1$ m, we obtained 29 roots: $\omega_1 = 2.62768$, $\omega_2 = 5.30732$, $\omega_3 = 8.06714$, ..., $\omega_{29} = 88.1904$. Generally 30 terms are more than sufficient to produce converging numerical solutions. We generated the standard Wiener process increments in Hilbert space for the time intervals of 0.001 days for the total time of 3 days. Then eigenvalues λ_n were computed for the required σ^2. With these roots, ω and λ_n, we have

then calculated the basis function in equation (8.20). Those values were used to generate $d\beta(t)$ in equation (8.15). The numerical scheme of SSTM was then used to calculate the concentration profile for spatial-temporal development for the mean velocity of 0.5 m/day. This value of mean velocity can be thought as large enough to have a sufficient plume development within a few days and small enough to depict the variability in concentration profiles.

We have used spatial grid length of 0.1 m for the numerical calculations. It can be shown by analyzing equation (8.14) mathematically, the grid size (h_x) less than 0.1 does not effect the solution significantly. Initial concentration value of 1.0 unit was considered at $x = 0$ and it was assumed as a continuous source for the entire time period of the solution. Exponentially distributed concentration values of $e^{-5k\Delta x}$, where $k = 1, 2, ...,10$ and Δx is the grid size, were considered as the initial conditions at the other locations.

To investigate the general behavior of the model, we have obtained the temporal development of the concentration profiles at the mid point of the domain ($x = 0.5$m) for various parameter combinations of b and σ^2. The same realization of standard Wiener process increments and constant mean velocity of 0.5 m/day were used for all the computational experiments.

First we will illustrate that the SSTM can mimic the solution of advection-dispersion equation. We have used the concentration profiles given by the stochastic model as the observations of solute concentration to estimate the appropriate hydrodynamic dispersion coefficient (D) of the advection-dispersion model by using a stochastic inverse method, which will be described in Chapter 10. Using the inverse method we can answer the question: what would be the approximate dispersion coefficient given the concentration profiles from the SSTM assuming that the deterministic advection-dispersion equation can be applied? In this way we can compare the SSTM with the solutions of the advection-dispersion equation for the same boundary and initial conditions. The parameters of the SSTM, $\sigma^2 = 0.001$ and $b = 0.0001$, gave the corresponding estimate of 0.01 m^2/day for D and the SSTM can represent the advection-dispersion model with the estimated D (Figure 8.4).
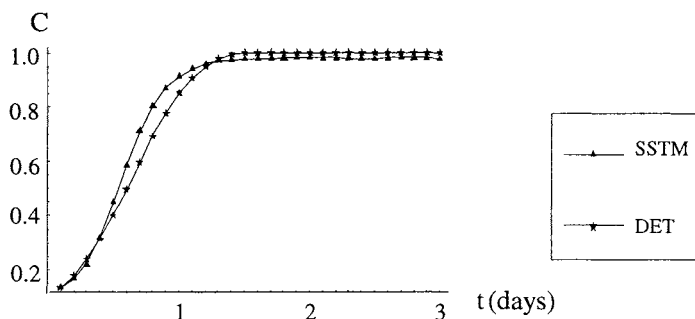
Figure 8.4   Comparison of deterministic ($D = 0.01$) and stochastic ($\sigma^2 = 0.001$ and $b = 0.0001$) model concentration profiles for 1 m domain.

Figure 8.5 illustrates that the SSTM could mimic the advection-dispersion model even for a larger scale, $0 \leq x \leq 10$ m, for the 30 day time period used in the calculation. We used the same SSTM parameters that were used in 1 m case and obtained the estimate
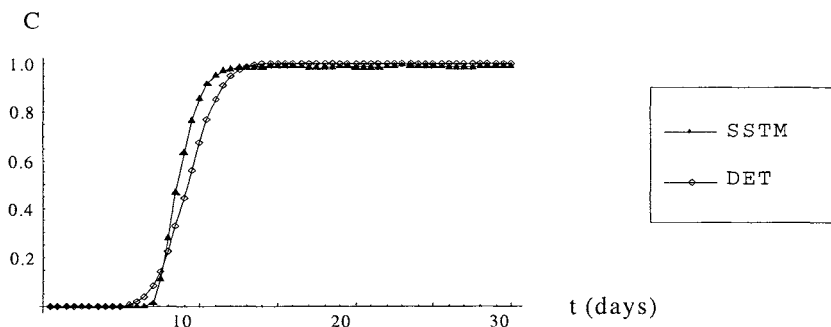of 0.037 m^2/day for D.

Figure 8.5   Comparison of deterministic ($D = 0.037$ m^2/day) and stochastic ($\sigma^2 = 0.001$ and $b = 0.0001$) model concentration profiles for 10 m domain.

We explored the changes of the statistical nature of the solutions with different b and σ^2. The behavioral change of the concentration breakthrough curves was examined by keeping one parameter at a constant and changing the other. Figure 8.6 shows the concentration profiles at $x = 0.5$ m of 1 m domain, for a smaller value of $\sigma^2(0.0001)$ when b varies from 0.0001 m to 0.25 m. The randomness of almost all five curves are insignificant, i.e. it is difficult to distinguish the different profiles. Although, range of b varies from 0.0001 to 0.25m (a change of 2500 times) the change of stochasticity is negligible for smaller σ^2. When σ^2 approaches 0, flow is advective and the dispersion is negligible.
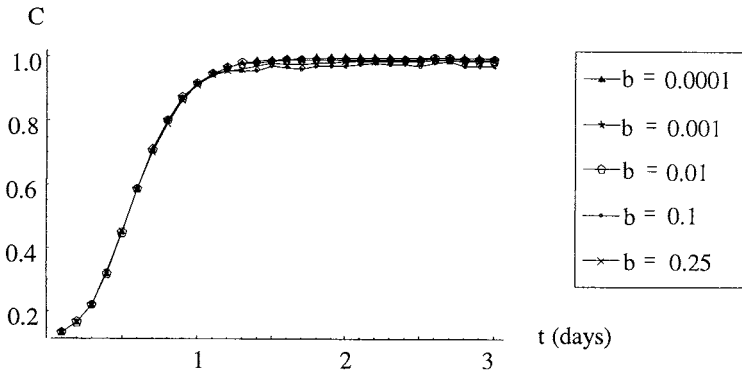
Figure 8.6   Concentration profile at $x = 0.5$m for $\sigma^2 = 0.0001$.

With the increase of σ^2 by 10 times for the same regime of b (0.0001 m to 0.25 m), Figure 8.7 shows visually distinguishable differences between concentration breakthrough curves. Furthermore, we can observe some curves have undergone notable stochasticity, especially when $b = 0.1$ m. The high values of variance not only directly increase the stochastic nature of the flow but also influence the ways in which b affects the flow. Another observation we can make from Figure 8.7 is that with the increase of stochasticity the concentration profile reaches its asymptotic value (sill) early and the maximum concentration value is less than those of more deterministic profiles.

C
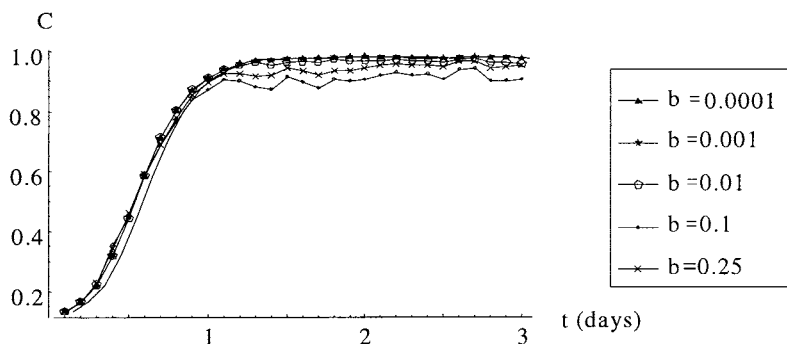
Figure 8.7   Concentration profile at $x = 0.5$ m for $\sigma^2 = 0.001$.

One can expect to see the increase of stochasticity with the increase of correlation length. When b is very small, flow is smooth and stable. However, it is interesting to see that, b at 0.1 m makes the concentration profile more variable. When b at a higher regime, 0.25m for example, the flow is less stochastic than it was at 0.1m. This may be caused by a sensitive range of b around 0.01 m. Figure 8.8 shows the concentration breakthrough curves for the similar b ranges at $\sigma^2 = 0.01$. Flow tends to be unsteady for larger correlation lengths; however, stochasticity of smaller b values is still trivial. Increase of σ^2 intensifies stochasticity and effect of b in the flow a great deal. The unpredictable behavior of the flow around 0.01 m of b shown in Figure 8.7 exists in current σ^2 as well.
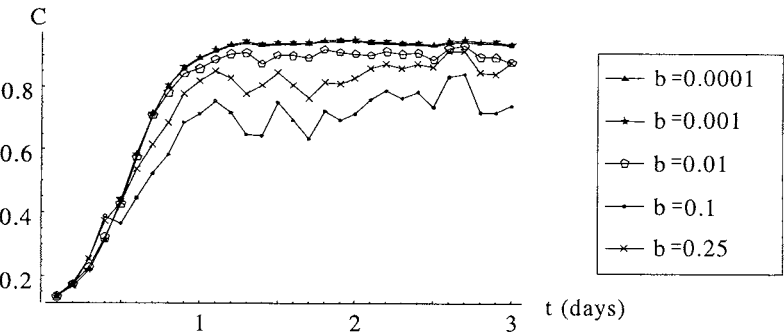
Figure 8.8   Concentration profile at $x = 0.5$ m for $\sigma^2 = 0.01$.

We extended the investigation by keeping b at a constant and changing σ^2. Figure 8.9 shows the concentration profiles at $b = 0.0001$ for varying σ^2 (0.0001 to 0.25). In Figure 8.6, small σ^2 demonstrates negligible stochasticity even for very high b values, whereas, in Figure 8.9, irrespective of smaller b, σ^2 influences the stochasticity of the flow. However, it is difficult to distinguish the concentration profiles for smaller σ^2 (0.0001 and 0.001). With the increase of σ^2 stochasticity increases rapidly. Therefore, we can assume that σ^2 is the dominant parameter which regulates the behavior of the flow.
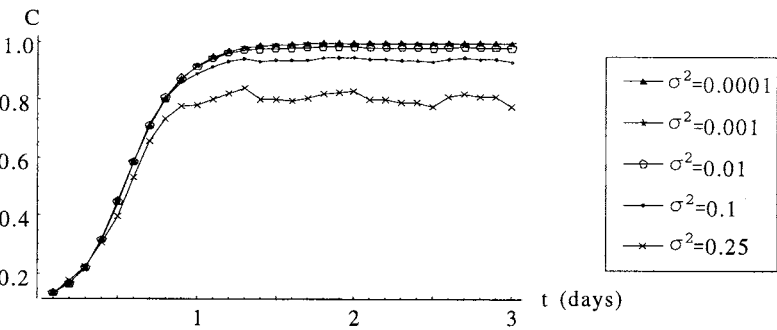
Figure 8.9   Concentration profile at $x = 0.5$m for $b = 0.0001$.

We increased b by 10 times and obtained Figure 8.10 which shows that randomness increases considerably.
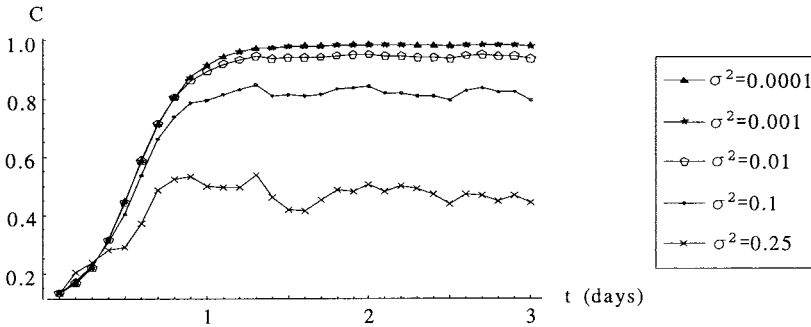
Figure 8.10. Concentration profile at $x = 0.5$m for b = 0.001.

It may be more appropriate and statistically sound to use confidence intervals rather than depend on a few realizations of the standard Wiener increments to understand the effect of σ^2. We used 50 different Wiener increments to calculate the 95% confidence intervals. Figure 8.11(a) clearly shows that for the smaller values of parameters ($\sigma^2 = 0.001$, $b = 0.01$), which represent less heterogeneity of the system, the variations of concentration profiles are negligible and hardly distinguishable. Figure 8.11(b) exhibits that when the parameter values are increased the stochasticity increases. The confidence intervals of Figure 8.11(b) demonstrate that the model is quite stable even for highly stochastic flow.
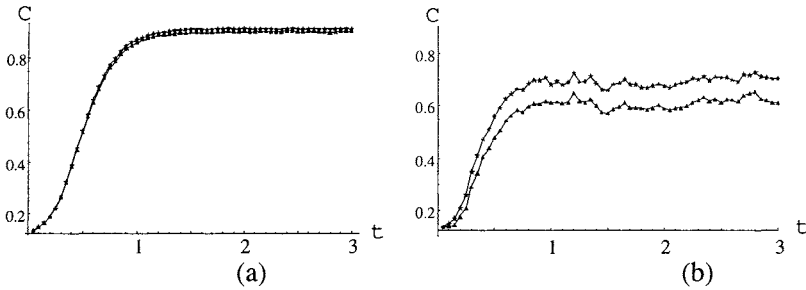
Figure 8.11   95% of confidence interval profiles with 50 different Wiener increments;   (a) σ^2=0.001, b=0.01 ;   (b) σ^2=0.1, b= 0.1.

We explored the effects of different random Wiener process increments. Figures 8.12 and 8.13 show the concentration profiles for five different Wiener processes for two different combinations of parameters. There are no considerable differences among these breakthrough curves, i.e. the influence of the Wiener process is minimal to the nature of the flow.
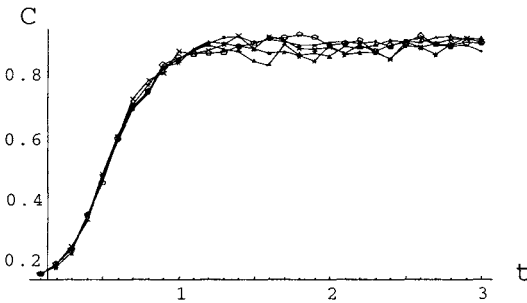
Figure 8.12   Concentration profiles for five different Wiener process increments at x = 0.5 m for σ^2 = 0.001 and b = 0.01.
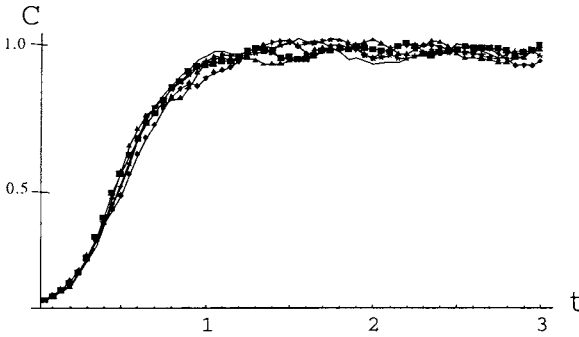
Figure 8.13   Concentration profiles for five different Wiener process increments at $x = 0.5$ m for $\sigma^2 = 0.01$ and $b = 0.1$.

8.6   Hypotheses Related to Variance and Correlation Length

Having understood some of the features of the model behavior, we can develop hypotheses about the parameters of the stochastic model relating to the physical phenomenon. As a fairly simple but reasonable attempt, it was hypothesized that the variance, σ^2, is a function of pore size and inversely proportional to the porosity ($\sigma^2 \propto (1/\varphi)$, where $\varphi =$ porosity). Low σ^2 represents larger pore sizes and more possible travel paths, i.e. solute can travel in water with fewer disturbances in less heterogeneous media. As a result, randomness of the travel paths and the occurrence of random mixing decrease. On other hand, larger σ^2 represents a medium of smaller pore size. Therefore, there are less straight travel paths and water tends to travel in various directions. This phenomenon can increase the mixing of the solute and, hence, increases dispersion and stochasticity.

We further hypothesized that the correlation length, b, is representative of the geometry of the pores. The small b represents the medium of isotropic and homogeneous formation, and larger b represents anistropic and heterogeneous porous medium.

When the pore sizes are fairly large the effect of the geometry is negligible. Flow paths can find easier ways through larger pores irrespective of the shapes of particles. Figure 8.6 shows that hypotheses are reasonable. Low σ^2,

0.0001, represents large pores, therefore the flow is stable for all the shapes of geometry (any *b* value). In the case of larger σ^2, where pore size is smaller, the geometry can play a vital role. Even though the effective pore size is smaller, if geometry of the pores are regular, particles could find a reasonably homogeneous paths and that comparatively reduces the random mixing of flow (Figure 8.7 and 8.8). In addition, the geometry and size of pores are interrelated in a complex manner.

We have also investigated the effect of parameters for the larger scales: 10 m, 20 m, 30 m, 50 m and 100 m (see Figures 8.14 to 8.17). Figure 8.14 and Figure 8.15 show that increase of stochasticity with σ^2 for 10 m domain. Comparison of Figure 8.14 and Figure 8.16 illustrate that σ^2 is the most dominant parameter and our hypotheses seem to be reasonable for larger scales as well.
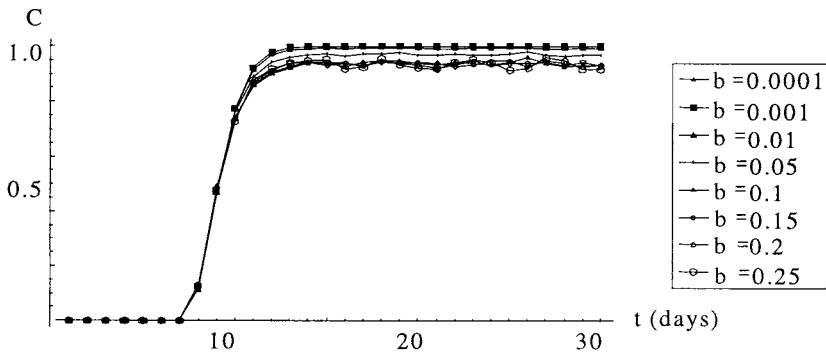
Figure 8.14   Concentration profile at x = 5m (of 10 m domain) for σ^2 = 0.0001.
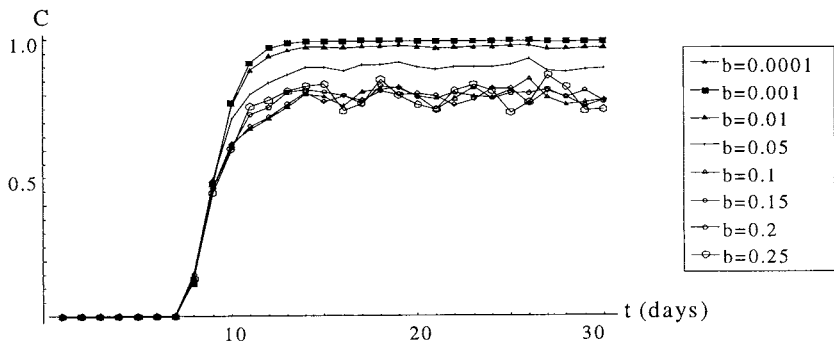
Figure 8.15   Concentration profile at x = 5m (of 10 m domain) for σ^2 = 0.001.
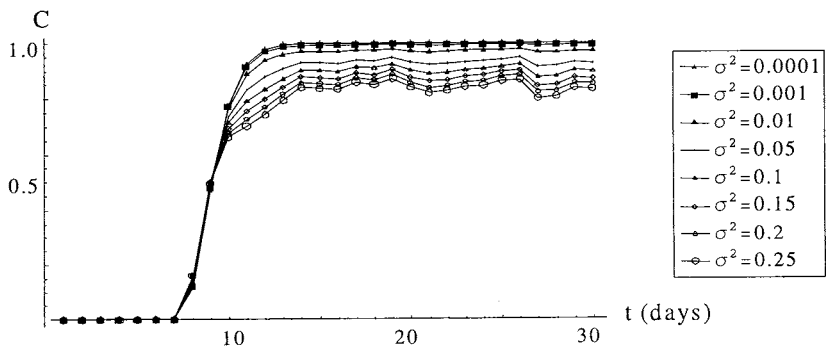
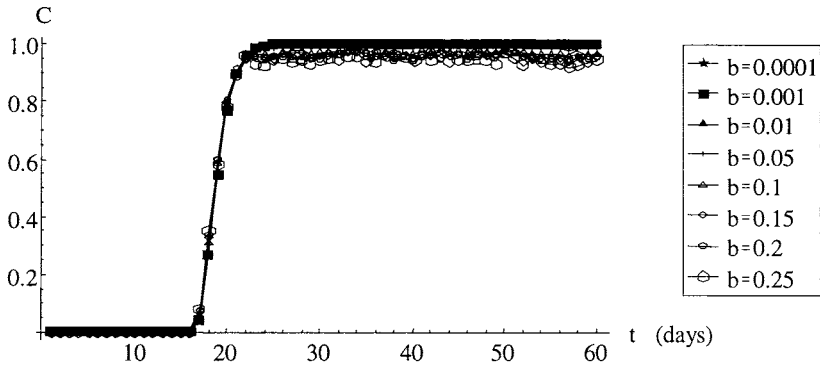Figure 8.16   Concentration profile at x = 5m (of 10 m domain) for b = 0.0001.

Figure 8.17   Concentration profile at $x = 10$m (of 20 m domain) for $\sigma^2 = 0.0001$.

8.7   Scale Dependency

As we have discussed in Chapter 1, the scale dependency of the hydrodynamic dispersion coefficient is an outcome of the associated Fickian assumptions. In developing the SSTM, we have not used any linearizing assumptions, but we have assumed a covariance kernel based on plausible arguments. It is reasonable to ask the question whether the parameters in the SSTM are dependent on the scale of the experiment. As the covariance kernel is based on the measures related to the properties of porous medium that are intrinsically affecting the flow, such as geometry of particle and pore sizes, we could expect low level of scale dependency in the case of the SSTM.

Comparison of Figure 8.6 and Figure 8.14 shows that stochasticity of the flow has increased with the scale of the experiment for the same parameters. Figures 8.7, 8.15, and 8.16 illustrate the same. Even though similar model performances are evident in other scales, visual comparison may not be sufficient to conclusively support capturing of scale dependency.

Can we observe the scale dependency of D by taking the concentration profiles from the SSTM as experimental observations and estimating the dispersion coefficient arising from the deterministic advection-dispersion equation? We employed the stochastic inverse method mentioned earlier to

estimate D by using concentration realizations of the SSTM. As Figure 8.4 and Figure 8.5 show, D has increased from 0.01 m^2/day to 0.037 m^2/day with the scale for same parameters. However, as will be shown later, the reliability of the estimates obtained from the stochastic estimation method reduces with the increase in stochasticity. Therefore, such estimation method may not be suitable to estimate parameters with highly stochastic flows where values of σ^2 and b are large. However, flow with low level stochasticity illustrates that the SSTM is capable of explaining the scale dependency of D, but this needs to be explored in more detail.

8.8   Validation of One Dimensional SSTM

The validation of a model is the process of comparing the appropriate outputs of a model with the corresponding observations of the real system. It is a common practice to compare the model performance against available accepted models, which we did by comparing the model with widely accepted and commonly used advection-dispersion model. Our investigation showed that the SSTM could mimic the deterministic advection-dispersion model with reasonable accuracy at the 1-D level. In this section, we compare the results of the SSTM with those of the contaminant transport tests conducted at large, confined, artificial aquifers at Lincoln University, Canterbury, New Zealand. Furthermore, we use this exercise as a primary step for understanding the issues relating to the aspect of practical application of the SSTM.

8.8.1 Lincoln University Experimental Aquifers

Lincoln University experimental aquifers (2 in number) are 9.49 m long, 4.66 m wide and 2.6 m deep. As shown in Figure 8.18 constant head tanks bound the aquifer at its upstream and downstream ends. A porous wall provides the hydraulic connection between the aquifer and head tanks. A weir controls the water surface elevation in each head tank, and each weir can be adjusted
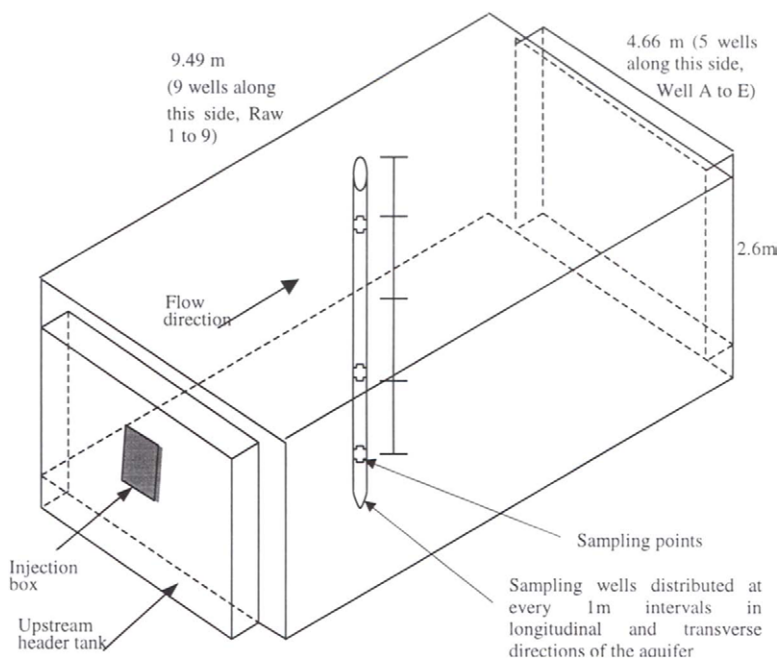

Figure 8.18   Schematic diagram of artificial aquifer at Lincoln University, New Zealand (Courtesy of Dr. John Bright, Lincoln Ventures Ltd.)

to provide different hydraulic gradients. However, the uniform hydraulic gradient of 0.017m/9.49m (= 0.0018) was maintained during the entire experiment. All other boundaries are zero flow boundaries. The aquifer media is sand.

Multi-port monitoring wells are laid out on a 1m x 1m grid. Computer controlled peristaltic pumps enable fully automated, simultaneous solute water samples to be collected from sample points that are uniformly distributed throughout the aquifer (four sample points for each grid point at 0.4m, 1.0m, 1.6m and 2.2m depth from the top surface of the aquifer). The tracer used was Rhodamine WT (RWT) dye with an initial concentration of 200 parts per billion and then allowed to decrease exponentially. Tracer was injected at middle of the header tank by using an injection box (dimensions of 50 cm length, 10 cm width and 20 cm depth). This tracer was rapidly mixed into the upstream header tank and thus infiltrated across the whole of the upstream face of the aquifer. The dye was injected at 12.00 noon and samples were collected at 2 to 4 hour intervals (however, there are some exceptions on time intervals) for 432 hours.

8.8.2 Methodology of Validation

Since, the present stochastic model is one-dimensional, we experimented with directly relating to solute concentration profiles in a single dimension of the aquifer. However, as one can assume, the actual aquifer is subjected transverse dispersion and consideration of mere one-dimensional flow is not sufficiently accurate. Therefore, we employed the following methodology to approximate the aquifer parameters.

There are solute concentration values of the artificial aquifer available for a large number of spatial points for different temporal intervals. Mainly the data are available for header tank, row 1, row 3, row 5, row 7 and row 9 (see Figure 8.18) for all the levels. First we selected few spatial coordinates at row 5 of well A – level YE. Then, we developed a two-dimensional deterministic advection-dispersion transport model and obtained corresponding concentration values from the model at the selected spatial locations of the aquifer. As the past studies show, we assumed that transverse dispersion coefficient is 10% of the longitudinal dispersion (Fetter, 1999). The mean velocity of 0.5 m/day was considered. Afterwards the profiles of both the aquifer and the deterministic model were plotted in one axis system to compare their similarity. This curve fitting technique was carried out in

association with trial and error exercises to determine a most suitable fitting of the curves by changing dispersion coefficient of the deterministic model.

8.8.3 Results

After investigating many combinations of parameters by trial and error, we found that the longitudinal dispersion coefficient at closer to 0.1 m^2/day is giving a reasonable fit (Figure 8.19). Following figures show a sample of results. We found that closest fit is given by longitudinal dispersion coefficient of 0.15 m^2/day, and the transverse dispersion is 0.015 m^2/day. For the simplicity, the concentration values of the aquifer were normalized.
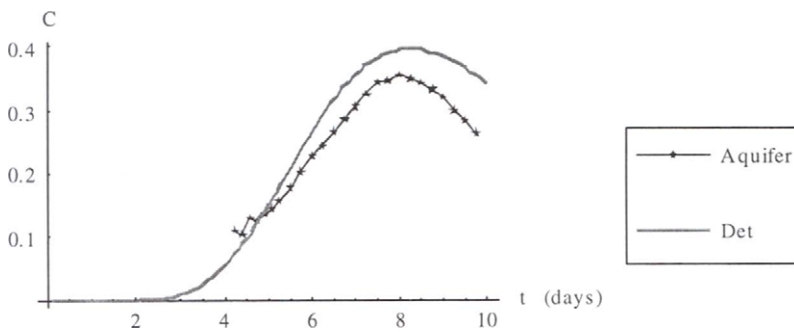
Figure 8.19   Concentration profile of trial and error curve fit for longitudinal dispersion coefficient of 0.1 m^2/day of advection dispersion model with row 5 of aquifer data.

However, the longitudinal dispersion coefficient of 0.15 m^2/day provides the best fit (see Figure 8.20).
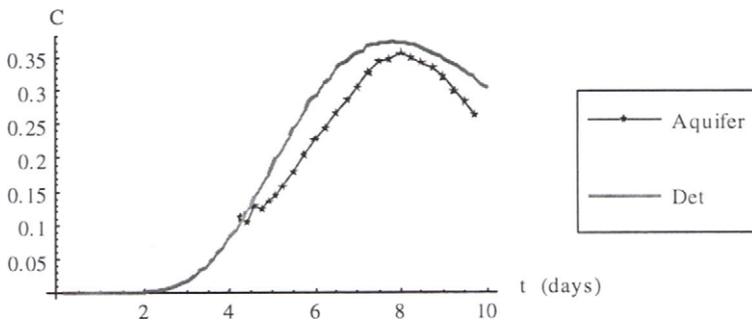
Figure 8.20   Concentration profile of trial and error curve fit for longitudinal dispersion coefficient of 0.15 m^2/day of advection dispersion model with row 5 of aquifer data.

Subsequently we developed a one-dimensional deterministic advection-dispersion model by using the longitudinal dispersion coefficient obtained from two-dimensional comparisons. As mentioned above, such a coefficient may be a more realistic representation of the artificial aquifer data transformed to 1-D. Then we used the same curve fitting technique that was used above, with the 1-D deterministic model and the 1-D stochastic model (SSTM). Investigation of curve fitting for different parameter combinations was conducted for the same Wiener process. The following are a sample of our trial and error curve fittings (Figures 8.21 - 8.24).
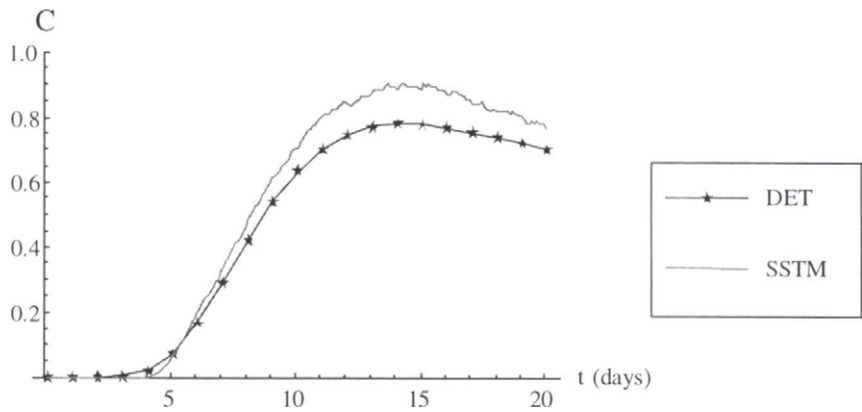
Figure 8.21   Concentration profiles of deterministic advection-dispersion model (D = 0.15 m^2/day) and SSTM with $\sigma^2 = 0.001$ and $b = 0.01$.
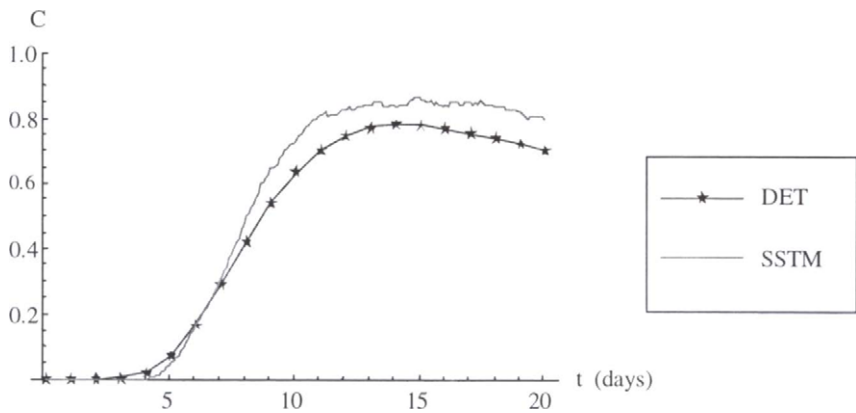
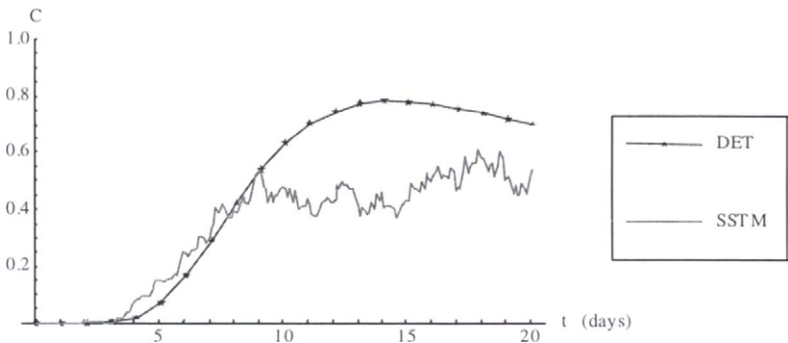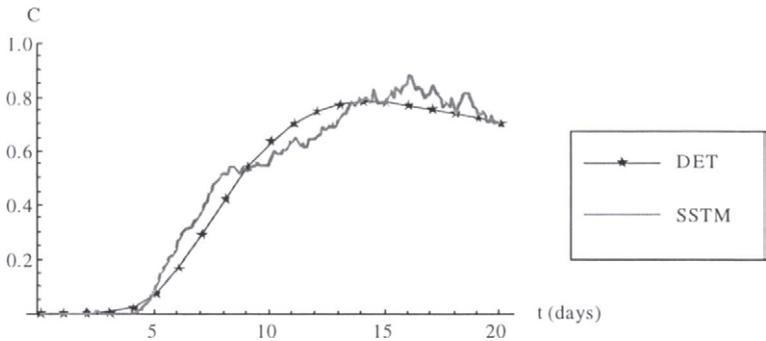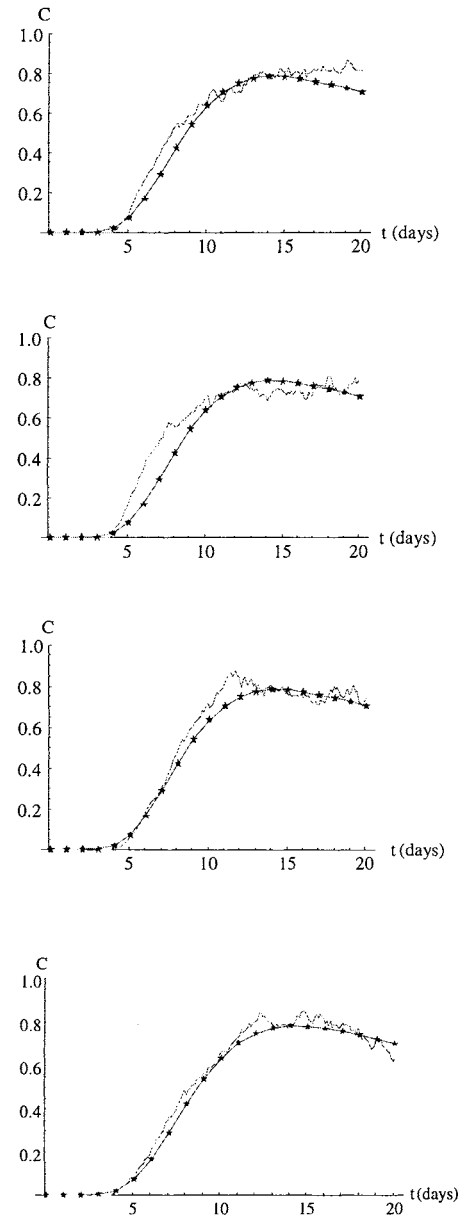
Figure 8.22   Concentration profiles of deterministic advection-dispersion model (D = 0.15 m^2/day) and SSTM with $\sigma^2 = 0.01$ and $b = 0.001$.

Figure 8.23   Concentration profiles of deterministic advection-dispersion model ($D = 0.15$ m^2/day) and SSTM with $\sigma^2 = 0.1$ and $b = 0.01$.

Figure 8.24   Concentration profiles of deterministic advection-dispersion model ($D = 0.15$ m^2/day) and SSTM with $\sigma^2 = 0.01$ and $b = 0.01$.

As figures 8.21 – 8.24 show parameter combination of the stochastic model that closely represent the aquifer data were $\sigma^2 = 0.01$ and $b = 0.01$.

Having determined the appropriate parameters of the SSTM that simulates the Lincoln University aquifer at a selected spatial location (Row 5 – well A) we investigated the robustness of the model for different Wiener processes. Figure 8.25 shows that model is reasonably stable for seven different sets of Wiener increments.
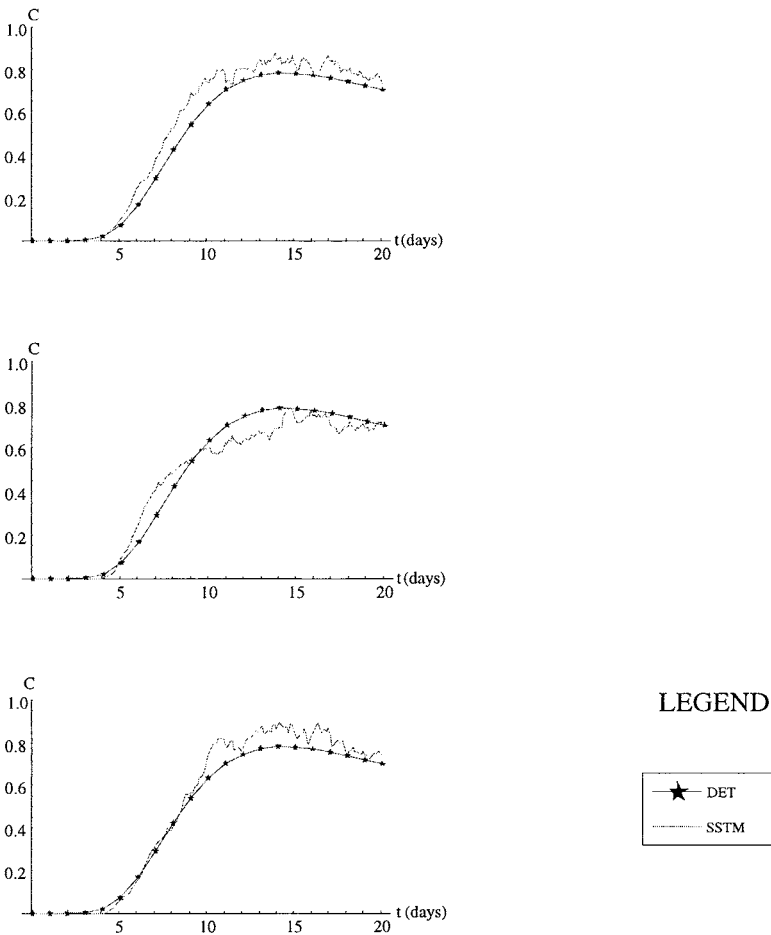
Figure 8.25   Concentration profiles of deterministic advection-dispersion model ($D = 0.15$ m^2/day) and SSTM with $\sigma^2 = 0.01$ and $b = 0.01$ for seven different standard Wiener processes.

Even though the above-mentioned results shows that parameter combination of $\sigma^2 = 0.01$ and $b = 0.01$ is a fairly accurate representation of the experimental aquifer for the given spatial point, we extended the validation

process for other spatial locations. Concentration data of row 3 of well A was considered. The methodology described in the previous section was applied for this data set as well. Figure 8.26 shows that 2-D deterministic advection-dispersion model with longitudinal dispersion coefficient of 0.15 m²/day reasonably fit the aquifer data for similar location.

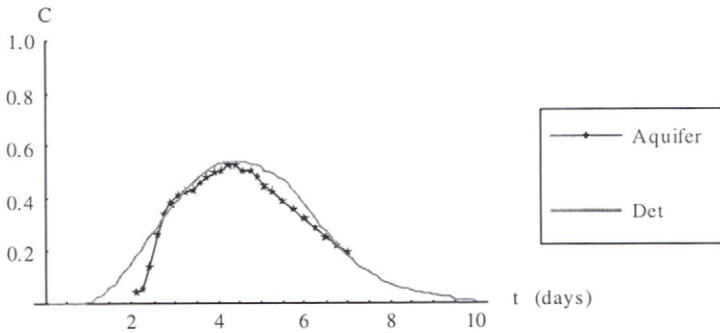Figure 8.26 Concentration profiles of 2D deterministic advection-dispersion model ($D = 0.15$ m²/day) and the experimental aquifer.

Since the given longitudinal dispersion coefficient is a plausible representation of the new spatial location, we continue the process into the next step to compare the curves of one-dimensional deterministic advection-dispersion model and those of the SSTM. We used the same parameters, $\sigma^2 = 0.01$ and $b = 0.01$, utilized in the above section for the present spatial point as well. Figure 8.27 shows that the curves of the deterministic model and SSTM are in a reasonable agreement.
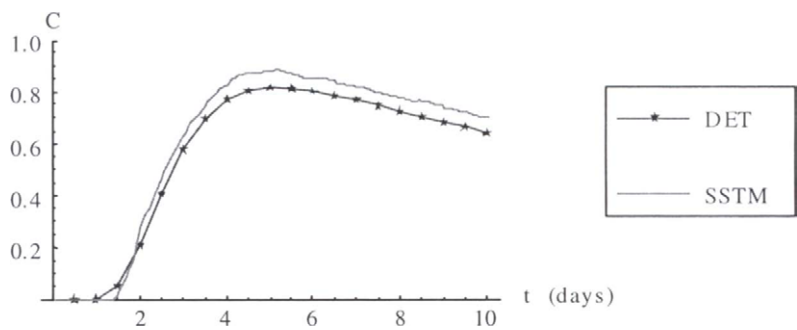
Figure 8.27   Concentration profiles of deterministic advection-dispersion model
($D = 0.15$ m^2/day and SSTM with $\sigma^2 = 0.001$ and $b = 0.01$ for row 3 well A.

We extended our comparison to row 7 of the same well. Figure 8.28 and
Figure 8.29 show that same parameter combination is reasonably valid for this
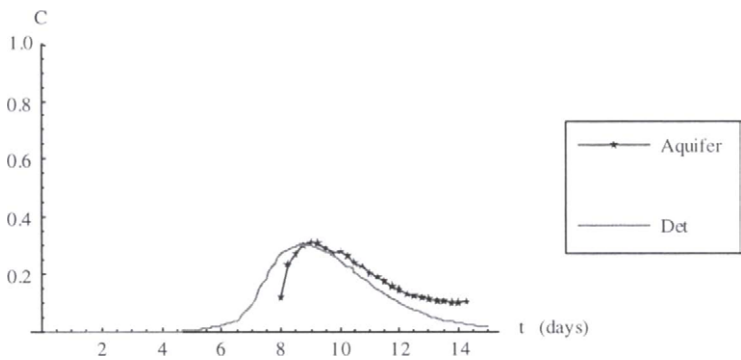spatial point as well.

Figure 8.28   Concentration profiles of 2D deterministic advection-dispersion
model ($D = 0.15$ m^2/day) and the experimental aquifer at row 7.

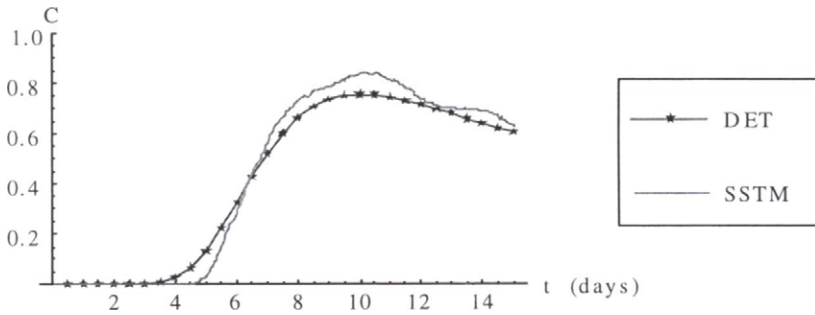Figure 8.29   Concentration profiles of deterministic advection-dispersion model ($D = 0.15$ m^2/day) and SSTM with $\sigma^2 = 0.001$ and $b = 0.01$ for row 7 well A.

8.7   Concluding Remarks

In this chapter we have developed a solute transport model using the concepts in stochastic calculus and tested the model using computations and comparing the outputs with the measured data from the artificial aquifer experiments. The new approach used to develop a stochastic solute transport model can be used to mathematically describe the dispersion without resorting to the Fickian assumptions. Even with a simpler covariance kernel for the velocity in 1-D, SSTM can produce satisfactory results with respect to the data collected from the aquifer. We have also showed that the parameters in the model could be related to the real aquifer properties but there is a lot to be done in that direction. Further research also needs to be done to characterize different kernels and the associated parameters based on currently available data from the experimental aquifers and natural underground formations.